Advances in Concrete Construction, *Vol. 17, No. 5 (2024) 257-271*
https://doi.org/10.12989/acc.2024.17.5.257

An intelligent cooling control system for mitigating the cracking risks of mass concretes during bridge construction

Ruinan An [1,6], Peng Lin*[1,2], Daoxiang Chen [1], Jianshu Ouyang [1,4], Zichang Li [2], Zheng Zhang [3] and Yuanguang Liu [5]

[1] *Department of Hydraulic Engineering, Tsinghua University, Beijing 100084, China*
[2] *Sichuan Energy Internet Research Institute, Tsinghua University, Chengdu 610213, China*
[3] *China Highway Engineering Consulting Corporation, Beijing 100089, China*
[4] *China Three Gorges Corporation, Beijing 100038, China*
[5] *Snohydro Bureau 11 Co. LTD., Sanmenxia 472001, China*
[6] *Rocket Force Academy, Beijing 100011, China*

(*Received February 1, 2024, Revised August 28, 2024, Accepted September 3, 2024*)

Abstract. During any construction involving mass concrete, it is crucial to control cracking during the placement and curing process. This study develops an intelligent cooling control system that regulates water temperature and flow based on concrete hydration heat, effectively preventing cracking in bridge construction. The system consists of hardware, a neural network-based control algorithm, and an information management system. An optimal cooling control strategy is proposed to dynamically regulate water flow and temperature, preventing cracking by utilizing real-time temperature data, target control curves, neural network algorithms, and cloud-based computing. The intelligent cooling control system has been successfully implemented in controlling cracking risks during bridge construction. It not only mitigates the risk but also provides a convenient management strategy for bridge construction projects. The optimal cooling control strategy ensures high accuracy and stability under unsupervised learning conditions. This intelligent cooling control system can be applied to similar constructions such as bridge, dam, and building that involve the use of mass concrete.

Keywords: bridge construction; cracking control; intelligent cooling system; machine learning; mass concrete

1. Introduction

Mass concrete have been widely used to construct bridges, dams and buildings at an unprecedented level nowadays. Unfortunately, the cracking of the mass concretes frequently occurs and results in shorter service life of concrete structures (Kim and Kim 1992, Li *et al*. 2023). As a matter of fact, it has always been a great challenge to prevent the cracking of the mass concretes. For example, the Quebec Bridge in Canada collapsed in 1907 due to concrete cracking and killed seventy-five workers (Pearson and Delatte 2006). The Silver Bridge in the United States collapsed in 1967 due to the deterioration of concretes (Feng *et al*. 2019). Subsequently, Federal Highway Administration initiated the National Bridge Inventory (NBI) inspection program to inspect all major bridges. A study by Krauss and Rogalla (1996) concluded that early transverse cracking had developed in about half of the concrete bridges surveyed by them (Krauss and Rogalla 1996).

The cracks in concrete bridges have led to higher maintenance costs. According to American Road & Transportation Builders Association (ARTBA), more than 45,000 bridges in the United States were in poor condition, which were classified as "structurally deficient (SD)". The average age of the SD bridges is about 68 years, compared to 32 years of the bridges in good conditions and 54 years of the bridges in fair conditions. It would take almost 40 years to repair the current backlog of the SD bridges with the cost of $41.8 billion (American Road and Transportation Builders Association 2021). Therefore, the cracking of concrete bridges has become a major technical problem in the bridge engineering and it is crucial to develop a cracking control technology to preventing the cracking, especially when mass concretes are involved in during the bridge construction.

Several scholars have conducted various studies on controlling the cracking of mass concrete bridges (García *et al*. 2013, Gilliland and Dilger 1997, Khan and Ali 2016). According to these studies, the essential factor resulting in the early concrete cracking is thermal stress (Subramaniam *et al*. 2010), two-third of which comes from cement hydration during the placing and curing of the concrete. The temperature change in mass concrete can be characterized by adiabatic temperature rise and temperature gradient (Bentz *et al*. 1998, Zhu *et al*. 2022). Various theoretical methods have been developed to predict the temperature change in concrete, with the Schmidt's method being the most used. However, these theoretical methods have been developed under ideal conditions and have certain limitations in engineering applications. Additionally, the

*Corresponding author, Ph.D., Professor,
E-mail: celinpe@tsinghua.edu.cn

ISSN: 2287-5301 (Print), 2287-531X (Online)

characterization of crack network geometry remains a difficult task due to the limitations inherent in experimental techniques (Sun *et al*. 2023).

With the rapid development of computation technology and numerical simulation software (e.g., ANSYS, MIDAS and ABAQUS), multi-parameter design is feasible for the mass concrete and the temperature distribution can be modeled accurately (Chuc *et al*. 2018, Tatro and Schrader 1985) although it is not until the recent few decades that the numerical simulation has been widely applied in engineering practices. Various engineering factors are considered in the numerical simulation, including location (Lawson *et al*. 2020), weather conditions (Song *et al*. 2016), structure design (Do 2015, Semendary *et al*. 2019, Wu *et al*. 2020), concrete age (Zhang *et al*. 2023) and material properties (An *et al*. 2020).

Moreover, advanced numerical, experimental, intelligent and machine learning techniques are implemented to predict the thermal stress in mass concrete and resultant cracking. In terms of the numerical techniques, the finite element method (FEM) was proved to be effectively simulate the development of concrete cracks under temperature stress (Li *et al*. 2014). A numerical simulation of underground culvert projects using the durability concrete model-complex three-dimensional (DuCOM-COM3D) analysis software was presented (Li *et al*. 2023). A new methodology for simulating post-cooling effect reduces the computational burden of FEM by replicating heat removal with fictitious convective boundaries (Conceicao *et al*. 2020). The crack-path-field and strain injection techniques enhance mesh independence in simulations (Dias *et al*. 2016), and its rheological simulations with a developed DEM hard-core/soft-shell model has simulated the flow of concrete and computed the macroscopic rheological behavior (Remond and Pizette 2014). According to experimental results, aggregate volume fraction and moisture condition of specimen are revealed as mainly affecting factors on the conductivity of concrete (Kim *et al*. 2003). Study results showed that increasing curing temperature causes an improvement in performance at an early age without penalizing its long-term properties (Djamila *et al*. 2018). An efficient experimental procedure with mechanistic thermal and structural analysis models was proposed to determine thermal stress and cracking in massive concrete structures when alternative, unconventional, or innovative concrete mixtures are considered for design (Chorzepa *et al*. 2018). A computer program was investigated as a useful tool to predict the overall thermal performance in developing thermal control plan (Sargam *et al*. 2019). The algorithms combining Jaya optimizer, Salp swarm algorithms and (least-squares) support vector machines were proposed to simulate the temperature effect in dam health monitoring modeling (Kang *et al*. 2019). The support vector machine regression (SVR) was utilized to establish the correlation between influencing variables and hydration heat temperature, thereby enhancing the accuracy of predicting effective hydration heat (Kang *et al*. 2019).

Besides investigating the thermal stress and cracking mechanisms of mass concrete as reviewed above, several studies have developed various cracking control measures, which mainly focus on two aspects: (1) controlling the temperature rise and differences in concrete blocks (Ning *et al*. 2022) and (2) improving structure design (e.g., mitigating structure restraints). The temperature control can be achieved by using low-heat cement (Crowley 2015, Ning *et al*. 2022), reducing cement ratio (Ng *et al*. 2017), substituting furnace slag and fly ash for partial natural sand (NS) and ordinary portland cement (Sahani *et al*. 2019), lowering concrete pouring temperature, applying insulation (Do *et al*. 2014) and implementing air cooled pipes (Azenha *et al*. 2014) and water-cooled pipes (Huang *et al*. 2018, Nguyen *et al*. 2019, Seo *et al*. 2015).

As one of the hot topics in the field of the bridge concrete cracking control, the water pipe cooling was proposed in 2005 and then extensively studied in the past decade in terms of developing monitoring methods, numerical simulation, thermal stress calculation, control theory and equipment system. The utilization of digital thermometers and fibers in concrete has become the prevailing approach for evaluating the performance of concrete structures (Khandel *et al*. 2021), thereby providing essential data support for further corporate research (Peng *et al*. 2020, Lin *et al*. 2021, Ning *et al*. 2022). Based on measured data, thermal properties of concrete were inferred and numerical analyses was conducted to verity the calculation accuracy (Yu *et al*. 2018), an inverse analysis method for adiabatic temperature rise function of concrete hydration heat was proposed using genetic algorithm and thermal analysis (Song *et al*. 2020). The closed-loop regulation theory was proposed in the field of intelligent control, leading to the development of an intelligent cooling control system in dam engineering (Lin *et al*. 2013). However, the comparison between bridge engineering and hydraulic engineering possesses its own distinct characteristics, resulting in certain disparities and challenges concerning the integration requirements of control standards, strategies and system.

Correspondingly, an intelligent cooling control system (ICCS) was developed in this study to control the cracking of the mass concrete during a bridge construction. The remainder of this paper is organized as follows. Section 2 introduces the development of the ICCS, which comprised a hardware system, a control algorithm based on the neural network model, and an information management system. A continuously iterating cooling control strategy was then proposed in Section 3 for on-site intelligent cooling control in the field applications. Section 4 applied the ICCS system to control the thermal stress and potential cracking of the mass concrete during the construction of the Sylla Mu Lun Grand Bridge in Inner Mongolia, China, which faced many challenges including high concrete strength, high insulation temperature, high reinforcement ratio, weak foundation restraint and concrete placement in cold weather. The performance of the intelligent cooling system in thermal cracking control was finally verified by the monitoring and control data.

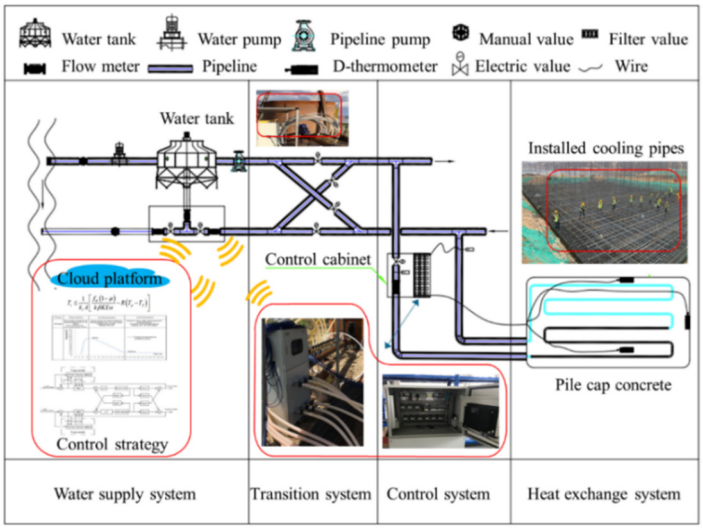

Fig. 1 Schematic diagram of the ICCS

2. Development of the ICCS

The bridge intelligent cooling system includes a hardware system for the water supply, recycling, commutation, control and heat exchange, a control algorithm based on the neural network model and an information management system.

2.1 Hardware development

The hardware of the ICCS includes the water supply and recycling, commutation, control, heat exchange systems (Fig. 1). In the closed-loop control model, the water-cooling temperature and flows are adjusted dynamically according to the concrete temperature. Multi-source data are collected via sensors and transmitted to the cloud, including installed water thermometer, flow meter, valve opening in cooling pipes, and hydraulic digital thermometers embedded in concrete. The electric T-valve device and pipeline pump are adjusted by the cloud platform, to achieve real-time control of the flow and temperature of the cooling system.

The water supply and recycling system mainly consists of the water tank, the water pump, the pipeline pump, the filter, and the electric T-valve device. A thermometer, a communication module, and a data acquisition device are used to collect and transmit water temperature in the water tank. Cooling water can be taken from nearby rivers. Pipe lines are suggested to be wrapped with thermal insulation material to keep the water temperature constant, and the electric T-valve device in the pipeline is equipped with a communication module and an electric valve. By regulating the recycled water flow into the water tank, the system interchanges the data with the cloud so as to control the water supply temperature.

The commutation system includes the crossing pipes and the electric valves installed between the water supply and recycling pipelines. The cooling water flow direction is changed with the temperature distribution in concrete by allowing periodic opening and closing of the four valves.

The control system is composed of an integrated flow and cooling temperature control cabinet and a cloud platform, as shown in Fig. 2. The control indexes include the highest temperature in concrete, the temperature difference between the interior and surface of concrete, the cooling rate, and the temperature difference between the cooling water and the concrete. Based on the multi-source data, the target temperature control curve, and the control algorithm, deep learning and online collaborative simulation are carried out in the cloud platform to select the optimal cooling control strategy. The integrated flow and temperature control cabinet collects multi-element data via sensors embedded in the branch pipelines, communicates with the cloud-based server, and receives cloud commands, including the electric valves, the embedded water thermometer and the flow meter. They change in a coordinated way, to meet the system requirements (i.e., $V_{T\text{-}Val}$, H_{pump}).

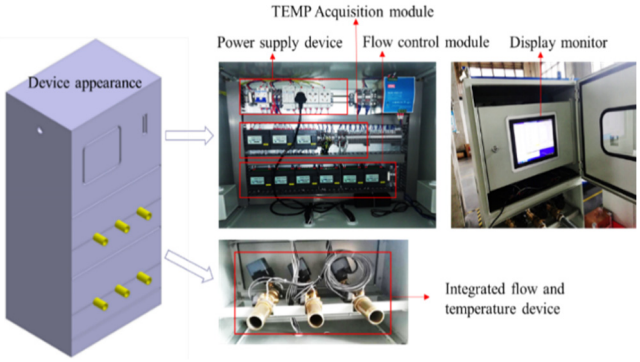

Fig. 2 Integrated flow and temperature control cabinet

The heat exchange system consists of the cooling pipelines and the hydraulic digital thermometers embedded in concrete. Several adjacent water supply pipes are installed, and the recycled water pipelines are connected directly to the main pipelines. Thermometers are installed inside and on the surface of concrete and connected to the integrated flow and temperature control cabinet.

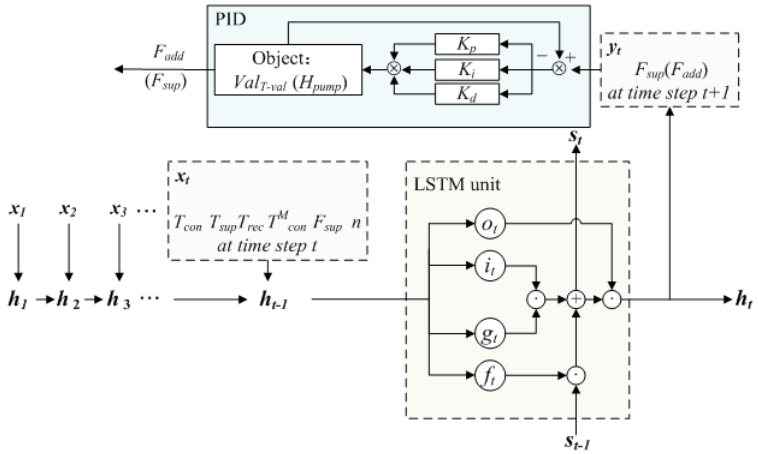

Fig. 3 Schematic control algorithm for ICCS prediction

2.2 Neural network model – based control algorithm

A dynamic mathematical algorithm was developed to control the cooling operation based on the neural networks of long short-term memory (LSTM) and a proportional-integral-derivative (PID) controller, as shown in Fig. 3. LSTM is a time-recursive neural network structure. The cell input information at the time t is composed of the input xt at the time step t and the output ht-1 at the time step t-1 to preserve the continuous information in the time dimension (Miao *et al*. 2023). Each cell is added with an input gate i_t, a forget gate f_t and an output gate o_t, and has the characteristics of learning sequential data, discovering their internal relations, and remembering data elements to well suit parameter prediction during the dynamic heat transfer process of the cooling system. By using LSTM, the optimal water supply and the recycled flow at time step $t+1$ can be quickly and accurately predicted through several temperatures and flow characteristic parameters that can be obtained at the time step t and complete the mapping from temperature to flow. It is also the basis for realizing the prediction of pump head and the adjustment of three-way valve opening by the PID controller, which can mitigate the accumulated errors for the concrete temperature control in the long-term prediction. The input of LSTM includes the concrete age (starting from the time of concrete placement) n_{age}, the internal concrete temperature T_{con}, the recycled water temperature T_{rec}, the cooling water supply temperature Tsup, and the supply water flow F_{sup} at the time t as well as the predicted values of concrete temperature T^M_{con} at time t+1. The output layer is the water supply F^M_{sup} and the recycled flow F^M_{add} at time t+1.

The PID controller is used to continuously adjust the proportional gain K_p, the integral gain K_i, and the derivative gain K_d so as to meet the temperature control requirements. However, these three parameters are nonlinear and cannot be well controlled by the conventional PID controller (Mohammadikia and Aliasghary 2019, An *et al*. 2024), especially with a long cooling water pipeline. The water-cooling system consists of many branch pipes and is subjected to continuous change of concrete thermal load, with evident lag and significant coupling problems. Therefore, a joint control strategy of LSTM and PID controller was established. The PID controller was used to reduce errors by adopting proportions, integrals and differentials, and LSTM was used to predict the parameters in the control system. By combining LSTM and PID controller, the influence of accumulated errors on the system accuracy can be eliminated in the long-term prediction. $Val_{T\text{-}Val}$ and H_{pump} in Fig. 3 indicate the T-valve opening and *the* water pump head, respectively, while $\odot$ denotes element multiplication and $\oplus$ denotes element addition. The control algorithm is shown in Eq. (1), in which $Val_{T\text{-}Val}$ determines the added water flow, and H_{pump} determines the water supply flow rate. These two parameters are adjusted together to vary the internal concrete temperature T_{con}.

$$\begin{aligned}&\left[T_{sup}(t), F_{sup}(t)\right]\\&= f\big(T_{con}(t-1), \dots, T_{con}\big(t-n_{age}\big),\\&\quad T_{rec}(t-1), \dots, T_{rec}\big(t-n_{age}\big), T_{add}(t-1), \dots,\\&\quad T_{add}\big(t-n_{age}\big), F_{sup}(t-1), \dots,\\&\quad F_{sup}\big(t-n_{age}\big), F_{rec}(t-1), \dots, F_{rec}\big(t-n_{age}\big)\big)\end{aligned} \tag{1}$$

where t is the time, $T_{sup}(t)$ and $F_{sup}(t)$ are the temperature and flow of cooling water supply at the time of t, $T_{con}(t-1)$ and $T_{con}\big(t-n_{age}\big)$ are the internal concrete temperature at the time of t-1 and t-n_{age}, nage is the concrete age starting from the time of concrete placement, $T_{rec}(t-1)$ and $T_{rec}\big(t-n_{age}\big)$ are the the recycled water temperature at the time of $t-1$ and $t-n_{age}$, $T_{add}(t-1)$ and $T_{add}\big(t-n_{age}\big)$ are the added water temperature at the time of $t-1$ and $t-n_{age}$, $F_{sup}(t-1)$ and $F_{sup}\big(t-n_{age}\big)$ are the flow of cooling water supply at the time of t-1 and $t-n_{age}$, $F_{rec}(t-1)$ and $F_{rec}\big(t-n_{age}\big)$ are the flow of recycled water at the time of t-1 and $t-n_{age}$.

The neural networks of LSTM and PID – based control algorithm was calibrated and verified by the experimental data of 13 bridge cap concrete with water cooling. Considering that a short control step triggers frequent

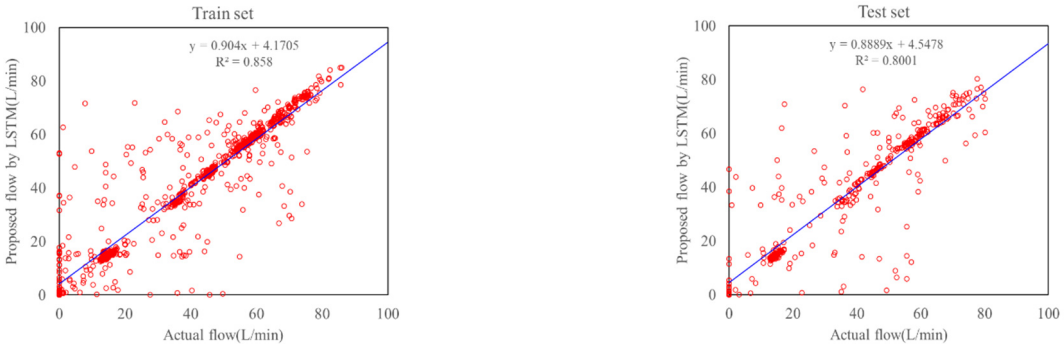

(a) The train set (b) The test set

Fig. 4 Data fit in LSTM model training

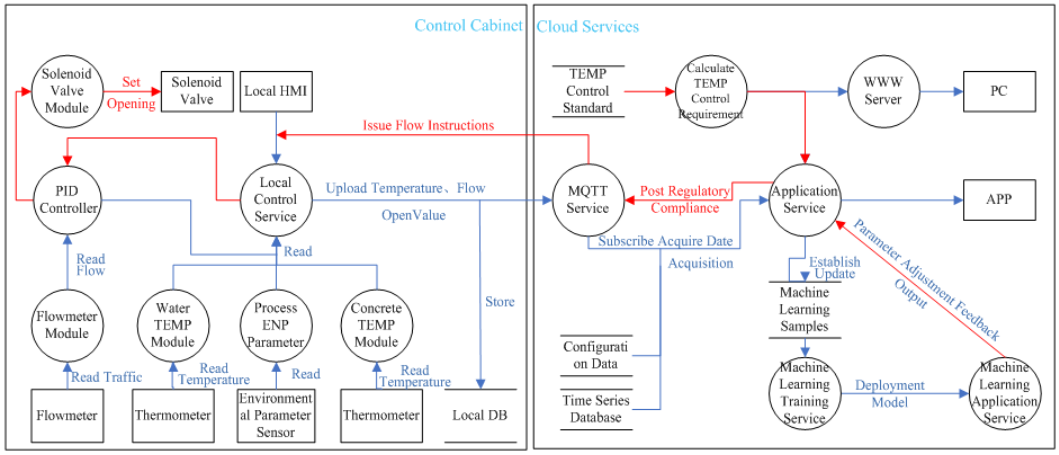

Fig. 5 Design and implementation process of the ICCS control model

control and increases algorithm complexity, an interval of 4 hours was used as the time step for flow prediction so as to balance the system complexity and control accuracy. The original data of 1,600 groups were sampled, including the concrete temperature T_{con} (ranging from 14.3 to 64.4°C), the water flow F_{sup} (0 to 86.0 L/min), the inlet water temperature T_{sup} (5.9 to 49.8°C), the recycled water temperature T_{rec} (11.6 to 49.9°C) and concrete age n_{age} (0.0 to 34.8 days).

For model training, 70% of the data were randomly selected as the training set and the remaining data as the test set. The mean absolute error (MAE) is taken as the loss function of the model, which is denoted as Eq. (2).

$$MAE = \frac{\sum_{i=1}^{n} |y_i - x_i|}{n} \tag{2}$$

where x_i and y_i are the predicted and actual flow values of the sample i. The mean absolute error is 3.81 L/min in the training set and 4.85 L/min in the test set. The actual flow and the recommended flow are compared in Fig. 4. The overall prediction error is lower than 5 L/min. The algorithm shows good linear data fit from the prediction set to the validation set.

The design and implementation process of the ICCS control algorithm was illustrated in Fig. 5. The ICCS control algorithm is used in two parts, namely edge computing and cloud computing. The edge computing part is encapsulated at the integrated control cabinet and logically includes two layers. The first layer is the perception layer (collecting data) including sensors and controllers while the second layer is the control services including the PID controller. As shown in the left diagram of Fig. 5, the measurement values recorded by the pressure gauges, flow meters, and inlet and outlet water thermometers are all acquired by the control service through the corresponding control module with Modbus protocol. The control service is then responsible for sending actuator commands and controlling valve opening degrees to adjust the flow rates. Standby operators can also check the sensor status and send the actuator commands through the human machine interface touch screen. The second part is the cloud-based computing off the site, as shown in the right diagram of Fig. 5, which logically composed of Message Queuing Telemetry Transport (MQTT) service for receiving reported data and issuing commands, Web application service for PC and App functions, database service for data storage, and service for machine learning training. As illustrated in Fig. 5, the two parts of the edge computing and cloud computing are connected through the operator network.

The current control requirements are calculated based on the gap between the target and present temperatures of the concrete. A machine learning service is then called to

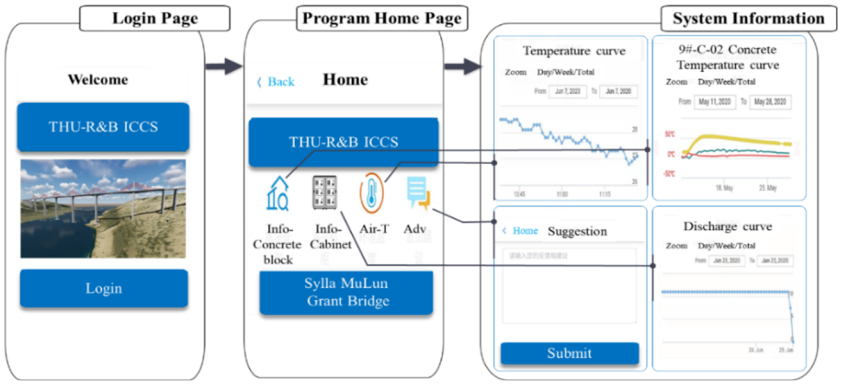

Fig. 6 The mobile terminal information platform for the ICCS

Table 1 Relevant provisions of concrete temperature control standards

JTG/T F50-2011 Technical Specification for Construction of Highway Bridge and Culvert	Pouring temperature: 5°C~28°C. Maximum temperature rise range: 50°C. Maximum internal temperature: 75°C. Maximum temperature difference between the center and the surface: 25°C. Maximum temperature difference between the fresh pouring and previous pouring layer: 20°C. Maximum temperature difference between inlet and outlet water of cooling pipes: 10°C. Maximum temperature difference between the cooling water and concrete: 20°C. Maximum concrete temperature daily drop rate: 2°C/day.
ACI207.4R Cooling and Insulating Systems for Mass Concrete	Pouring temperature: each 10 F (6°C) below the average air temperature will result in a lowering of the maximum temperature in concrete by about 6 F (3°C). Cooling time: should be continued for 1 to 2 weeks after peak temperature until the first of these conditions occur: a) The concrete cooling rate reaches the maximum that can be tolerated without cracking; b) The temperature of the concrete decreases to about 30 F (17°C) below the initial peak value. c) The concrete has been cooled to its final stable temperature or an intermediate temperature prescribed by the designer. Cooling rate: not exceeding 1 F (0.6°C) per day; 2 F (1°C) per day can be tolerated for a short period of time. Cooling should be resumed when the concrete temperature exceeds the initial peak temperature and is predicted to continue to increase to unacceptable levels.

acquire the current flow value setting and the flow value is given through the MQTT channel. The setting flow value is then obtained by utilizing the MQTT subscription function and sent to the PID controller. After that, the valve opening is adjusted according to the measured flow feedback from the PID loop, of which the parameters K_p, K_i, and K_d, are corrected by LSTM.

2.3 Information management platform

For the ICCS software system, a mobile information control platform (Reinforced Concrete Bridge Intelligent Cooling Control System developed by Tsinghua University, THU-R&B ICCS.) has been developed based on WeChat App, which can provide program-running stability and a user-friendly interface (Fig. 6). The broad coverage of wireless networks and the popularization of intelligent mobile devices provide hardware support for mobile monitoring operations. Widely-used WeChat App secures user login information, which simplifies the login procedures and improves the user experience. The information about the heat exchange system (i.e., concrete temperature, water temperature, and water flow) is fed into the software system and timely transmitted to supervisors and managers.

The home page provides information on each single concrete block, temperature control cabinet, air temperature, and suggestions. Users can access the detailed information pages by clicking on the module links. The detailed information pages display all the parameters monitored by the temperature control system. For instance, when users select a concrete block, the information can be displayed in either curves or tables. By clicking different tabs, users can switch among data modules and see the details below the page.

3. Optimal cooling control strategy

The optimal cooling control strategy is developed to support the ICCS and is a temperature progressive-control framework, which composes of the requirements by experience-based standards, the numerical simulation and the automatic control based on data mining.

3.1 Requirements by experience-based standards

It is the most basic requirement for any engineering designs to satisfy the design standards, and it is essential to follow the engineering experiences and industry design

habits. The temperature control standards for mass concrete differ for various engineering structures, environmental conditions, and concrete materials (Table 1).

For example, the requirements of pouring temperature are no more than 32°C in the United States, 30 to 35°C in the former Soviet Union, no more than 30°C (Japan Civil Engineering Society) or 35°C (Architectural Institute of Japan) in Japan, and no more than 30°C (for deep foundations) or 28°C (for hydraulic structures) or 25°C (for electric power facilities) in China.

According to the Chinese Highway Engineering, ACI (American Concrete Institute) and ASTM (American Society for Materials and Testing) standards, the existing temperature control methods can be summarized into the following three categories: material pre-cooling, embedded pipe cooling, and ambient cooling. As can be seen from Table 1, these standards focus on controlling the maximum temperatures and the cooling rates, instead of the cooling time. For example, the ACI standards specify the provisions on the concrete temperature, the temperature rise, the artificial cooling rate of mass concrete but the thermal cracking in mass concrete bridges is not considered. As such, the engineering designers have to resort to other related specifications or codes.

3.2 Numerical simulation

Numerical simulation can be performed to optimize the design, ensure that the concrete temperature control effect meets the standards and develop the target temperature control curves. It considers the water volume and the concrete temperature limits and determines the most efficient and economical cooling pipe configuration under various working conditions.

The amount of cooling water and (or) the water temperature is adjusted to ensure that the predicted real-time temperature falls on the target curve during the construction. It is expected that the actual concrete temperature and the temperature difference will fluctuate along the target curves. The advantages of setting such target curves are as follows: (1) defining the initial expectations of the temperature evolution, (2) urging the system to be temperature-orientated instead of control measures, and (3) providing the basis for the ICCS.

3.3 Intelligent temperature control

The numerical simulation was combined with the cloud-based serving, artificial intelligence, and data mining to develop an intelligent temperature control method. It makes full use of the large databases based on automation control technology and monitoring data. A cyclic process includes the raw data collection, database processing, data mining by various algorithms, intelligent optimization of the target temperature control curve, intelligent prediction of the actual temperature control curve, and feedback of the heat transfer measures. Accurate analysis and continuous optimization can significantly improve the temperature control efficiency and reduce the cracking risk. The corresponding monitoring system is the premise to ensure

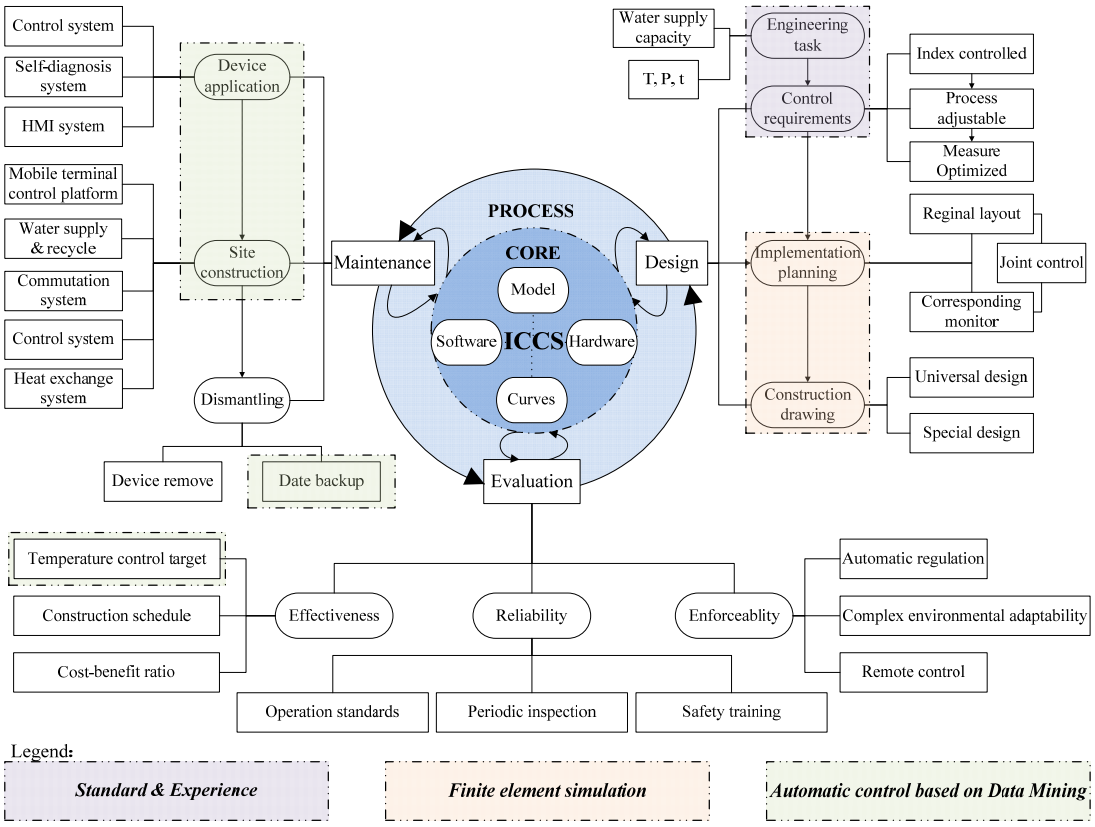

Fig. 7 The field temperature control procedures for the BICS

the database with enough data, constant updates, and high accuracy.

3.4 Progressive temperature control framework

The water-cooling control methods based on the experience-based standards, numerical simulation and data mining are integrated in this study. Fig. 7 depicts the framework of the progressive temperature control developed by utilizing the integrated ICCS, which involves in the design, installation, operation, monitoring and system evaluation. The temperature control procedures can be described as: (1) A preliminary design is conducted based on the experience and customary practices following the design standards and regulations. (2) The execution plans of piping installation are modeled and verified via the numerical simulation. (3) In the operation stage, the intelligent control algorithm is adopted to develop a strategy for automatic operation of the water-cooling system. It is a design and optimization procedure to guide the construction operation and to improve intelligent management.

(1) Basis for intelligent control

The core basis for the intelligent control includes the control curves, models, hardware, and software. The control curves set the concrete temperature boundaries to be followed throughout the project construction process. Different from the conventional practice of only specifying the thresholds of the important indicators in the standard, the intelligent control proposed in this study follows the principle of reducing the cooling gradient and slowing down the cooling rate, which can accurately control the temperature at each moment, and draw a continuous temperature control curve to achieve stricter temperature control than that in the specification. The stricter temperature control includes the maximum temperature of 70.5°C, the maximum difference between the temperatures at the center and surface of 23.5°C, and the daily decrease of 1.5~2.0°C/d. At the same time, the index of the control deviation is set to evaluate the degree of agreement between the actual and target temperature control curves. The control models ensure the proper operation of the water-cooling system (i.e., water temperature, flow quantity, and flow direction) so as to prevent any concrete cracking. When the control hardware is being selected, the high-quality performance, safe and smooth operation, and relatively low capital investment are the critical factors to be considered. The control software is the human-machine interface developed to provide a remote monitoring platform.

(2) Three stages

Design, operation and evaluation are the three typical stages for the temperature control. Based on the intelligent temperature control procedures proposed in this paper, each stage has independent feedback and can be updated and optimized via concept innovation and technological advancement. The three stages also support and promote each other. For example, the design stage involves in the stages of the on-site construction and engineering evaluation. The on-site construction stage is based on the design and needs to consider the evaluation criteria to achieve self-restraint. The evaluation stage can help to improve the design and construction quality. Notably, the evaluation should be based on the engineering practices and feedback to the design and construction

(3) Procedures

The three stages of the field temperature control procedures are analyzed in the following paragraphs based on the multi-source perception, real-time analysis and intelligent control.

In the design stage, the temperature control requirements, construction drawings, and implementation plans, sequences and schedules shall be considered. With the characteristics of the water-cooling system (i.e., water temperature, pressure, and water supply capacity) in the mind, the temperature control requirements are formulated, which include the controllable indexes, adaptability in the stages, and optimization of the cooling operation. The implementation plan includes the layout of the water pipes and monitoring sensors following the principles of the sub-regional layout of the monitoring equipment to provide the joint monitoring and pre-control, if possible. For the construction drawings, attentions should be paid to the general design of modular construction, and the special design should be considered for complicated structural parts or extreme conditions.

The operation stage includes the equipment application as well as the system installation, operation and dismantling. More efforts are needed to improve the intelligentization level of the system and avoid the human interference in the system adjustment, self-diagnosis and human-machine interacting systems. In terms of the system installation, the capacity, safety, convenience and cost control shall be ensured for the water supply and recycling system. The location of the cooling water pipes should be precisely positioned. The monitoring platform can visually display historical data queries, water supply performance, early warning, and temperature as well as flow control.

In the evaluation stage, the evaluation indexes include the temperature control effectiveness, safety reliability, and technical feasibility. The matching degree of the temperature control and construction technology, the probability of completion on schedule, and the investment to return ratio are evaluated for the effectiveness of the intelligent temperature control. Regarding the safety reliability, a system is established to standardize the operation of the control system, periodic inspections of equipment safety and safety training. In terms of the technical feasibility, the ability of automatic updating, the adaptability to complex construction environments and the ability of remote control are evaluated.

4. Case study on the application of the ICCS

4.1 Sylla Mu Lun Grand Bridge

The Sylla Mu Lun Grand Bridge is located on the Danxi Highway between Keshketen and Chengde as a part of the national highway network in China. The highway on the bridge has two-way four-lane while the bridge has a total

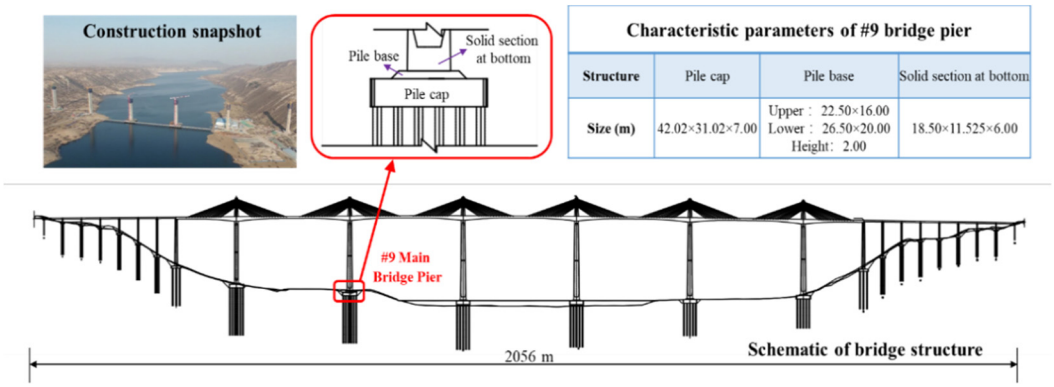

Characteristic parameters of #9 bridge pier			
Structure	Pile cap	Pile base	Solid section at bottom
Size (m)	42.02×31.02×7.00	Upper： 22.50×16.00 Lower： 26.50×20.00 Height： 2.00	18.50×11.525×6.00

Fig. 8 Profile and characteristic parameters of Sylla Mu Lun Grand Bridge

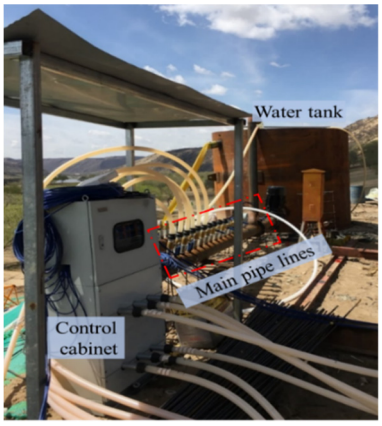

(a) Water supply and control system

(b) Cooling pipes outside the concrete block

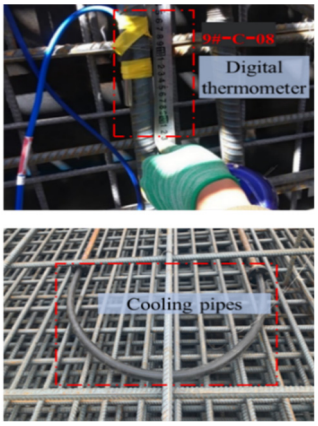

(c) Cooling pipes and thermometers in the concrete block

Fig. 9 Snapshots of bridge cooling control system

length of 2,064 m and is supported by the piers up to 160 m high. The bridge is composed of a main bridge and an approach bridge. The main bridge is a rigid frame system with a tower pier beam, as illustrated in Fig. 8. The piers are constructed with mass concrete on the pile foundation. C40 concrete (with 28-day compressive strength of 40 MPa) is used for the pier cap while C50 concrete for the pier base and shaft.

4.2 System installation

ICCS is applied in the mass concrete of 8 bridge piers, which has been in continuous use for 13 months, accumulating a large amount of monitoring data, and the system installation of the pier cap 9# taken as an example. It includes the water supply and recycling system, the flow control system, and the heat exchange system as illustrated in Fig. 9. The water supply pipes in the concrete block are DN40 iron pipes, and the intermittent period of the silo casting is seven days. The maximum cooling time is 30 days, the maximum water flow rate is 90 m^3/h and the flow rate is 100 m^3/h with the head loss taken into consideration. The water recycling system is similar to the water supply system. It collects the return water from the concrete blocks and discharges it into the river. Based on the calculated flow rate, the inner diameter of the water supply pipes is 150 mm. The system includes 18 bifurcated branch pipe systems, and the total length of a single water supply system is 4,014 mm.

The maximum water supply flow for one pier is 100 m^3/h, and the design volume of the water tank is 10 m^3 to allow dynamic pumping, water supply and recycling. The water tank is 2 m long, 2 m wide and 2.5 m high. The design pump head is 92 m based on the height difference between the pump location and the tank top. The location of water intake should be set in the middle of the river with deeper water and less siltation.

The commutation device can regularly change the pipe flow direction so as to avoid the inlet water temperature being significantly lower than that of the return water. The commutation device consists of a booster pump (25 m to 40 m head) and four manually-controlled reversing valves.

The integrated flow and temperature control cabinet is placed near the mass concrete block. Its functions include uploading the collected temperature data to the cloud and executing the flow and temperature adjustment commands. The cabinet is miniaturized, standardized, modularized, and composed of the control and cooling models. The cabinet integrates the wiring device, the acquisition module, the power supply module, the communication module and the central processing module. On one hand, it shortens the execution time of the temperature control instruction and

improves the efficiency of cooling water regulation. On the other hand, the cabinet is small with flexible mobility and diversified in quantity and combination according to the project needs. The modules can be replaced integrally and conveniently in of cabinet repair.

The heat exchange system includes the embedded water pipes and the thermometers. During construction of the pier cap, four layers of 880 m long cooling water pipes were installed with a vertical spacing of 1.75 m and a horizontal spacing of 1.5 m. At the same time, the temperature was measured by thermometers to ensure the actual average temperature inside the concrete, which were installed in the middle of two adjacent cooling water pipes.

4.3 Temperature control curves

The target control curves for the construction of the pier cap 9# in summer were taken as an example. A particular safety factor was reserved for various conditions considering the most economical and convenient construction. The temperature control path was determined and divided into the temperature controlling, dropping and stabilization phases.

(1) Material parameters

The thermal properties of the concrete are estimated based on the weight percentage of each component, by using Eqs. (3)-(5) (Vytenis 1994).

$$c = 1.05\left(p_c c_c + p_f c_f + p_w c_w + p_s c_s + p_g c_g\right) \quad (3)$$

$$\lambda = p_c\lambda_c + p_f\lambda_f + p_w\lambda_w + p_s\lambda_s + p_g\lambda_g \quad (4)$$

$$a = \frac{\lambda}{c\rho} \quad (5)$$

where p_c, p_f, p_w, p_s and p_g are the weight percentage of the cement, fly ash, water, sand and gravel in the concrete, respectively. c, c_c, c_f, c_w, c_s and c_g are the specific heat of the concrete, cement, fly ash, water, sand and gravel, respectively. λ, λ_c, λ_f, λ_w, λ_s, and λ_g are the thermal conductivity of the concrete, cement, fly ash, water, sand and gravel, respectively. ρ and a are the concrete density and the concrete heat transfer coefficient, and the values of the parameters are shown in Tables 2 and 3.

The adiabatic temperature rise can be estimated according to the cement hydration heat and fitting the hydration heat curve as shown in Eq. (6) (Vytenis 1994).

$$Q(\tau) = Q_0[1 - exp(-a_1\tau^{b_1})] \quad (6)$$

where $Q(\tau)$ is the accumulated hydration heat during the concrete age, and Q_0 is the final hydration heat when τ is infinity. For P.O 42.5 cement, $Q_0 = 330$ kJ/kg, $a_1 = 0.69$, and $b_1 = 0.56$ are taken as constants.

(2) Boundary conditions

The temperature and surface heat transfer coefficients on the boundary are known by setting the concrete surface as atmosphere. The atmospheric temperature fits the annual mean temperature function, as shown in Eq. (7).

$$T_a = T_{am} + A_a \cos\left[\frac{\pi}{6}(t - t_0)\right] \quad (7)$$

where T_a, T_{am} and $A_a$are the air temperature, the average annual temperature and the annual temperature amplitude, respectively. t_0 is the time corresponding to the highest temperature.

The water temperature changes with the ambient temperature and the relationships between the temperature, depth and time are expressed in Eqs. (8)-(11).

$$T(y,t) = T_m(y) + A(y)\cos\omega\,[t - t_0 - \varepsilon(y)] \quad (8)$$

$$T_m(y) = c + (T_s - c)e^{-\alpha y} \quad (9)$$

$$A(y) = A_0 e^{-\beta y} \quad (10)$$

$$\varepsilon(y) = d - fe^{-\gamma y} \quad (11)$$

where $T_m(y)$, $A(y)$and $\varepsilon(y)$ are the average annual water temperature, the annual water temperature amplitude, and the phase temperature difference between the water and the air at any depth, respectively. The parameter values in equations (9)-(11) are obtained through fitting the monthly average water temperature changes at the representative depth in the river, with the values being $c = 15.73$, $T_s = 9.7$, $A_0 = 11.75$, $d = 2.15$, $f = 1.3$, $\alpha = 0.04$,

Table 2 Weight Percentage and thermal Properties of Concrete C40 and C50

Concrete grade	p_c %	p_f %	p_w %	p_s %	p_g %	ρ kg/m^3	c kJ/(kg·°C)	λ kJ/(m·d·°/C)
C40	11.7	5.1	6.4	34.5	42.2	2454.5	0.98	178.6
C50	17.1	3.0	6.4	31.5	41.7	2437.9	0.96	175.3

Table 3 Thermal properties of concrete components

c_c kJ/(kg·°C)	c_f kJ/(kg·°C)	c_w kJ/(kg·°C)	c_s kJ/(kg·°C)	c_g kJ/(kg·°C)
0.456	0.92	4.187	0.699	0.766
λ_c kJ/(m·h·°C)	λ_f kJ/(m·h·°C)	λ_w kJ/(m·h·°C)	λ_s kJ/(m·h·°C)	λ_g kJ/(m·h·°C)
4.446	0.828	2.16	11.129	6.891

Table 4 Pipe cooling schemes in the initial design

Case	Pipeline layout		Water supply duration (d)	Material
	Vertical distance (m)	Horizontal spacing (m)		
1	No water-cooling measures			
2	1.25	0.5	60	Iron
3	1.25	1.0	60	Iron
4	1.875	0.5	60	Iron
5	1.875	1.0	60	Iron
6	1.25	1.0	60	HDPE

$\beta = 0.018,\ \gamma = 0.085.$

(3) Initial design

The model is established for the pier and divided into meshes. The equivalent negative heat source method is used to calculate the temperature change in the concrete. The casting temperature is 18°C, the diameter of the cooling water pipe is 48 mm, and the maximum water flow is 4 m^3/h. The pipes are made of either iron or high-density polyethylene. The vertical spacing between the cooling pipes is set to be either 1.25 m or 1.875 m, and the horizontal spacing is either 0.5 m or 1.0 m. The initial plan includes six schemes as shown in Table 4.

(4) Target curve

Based on the numerical simulation results (Fig. 10), the maximum concrete temperatures for Cases 1 to 6 are set to be 59.92°C, 41.57°C, 45.56°C, 48.79°C, 51.46°C and 47.92°C, respectively. The smaller the spacing of the cooling water pipes is, the sooner the maximum temperature drops and the lower the maximum temperature is. In Cases 1 and 2, the temperature difference between the neighbouring layers exceeds the limit range and thus does not meet the requirements. In Case 5, the temperature difference between the centre and surface is close to the limit in the standard, which, however, has exceeded the requirements of the target temperature control curves and does not satisfy the safety margin. Cases 3 and 4 meet the temperature control requirements, and the construction volume of Case 4 is 1.2 times of that of Case 3. Therefore, Case 3 is the most suitable compared to the other schemes.

Cases 3 and 6 compare the effects of pipe materials on water cooling. The maximum temperatures are 45.56°C and 47.92°C for Cases 3 and 6, respectively. The interior and surface temperature differences are 18.1°C and 20.32°C, respectively. The temperature differences of the

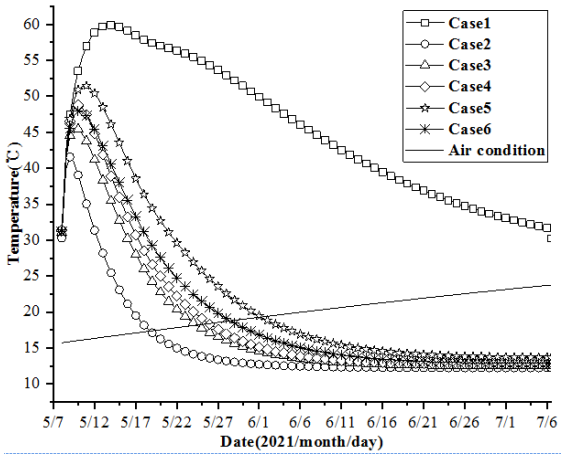

(a) Temperature of central concrete

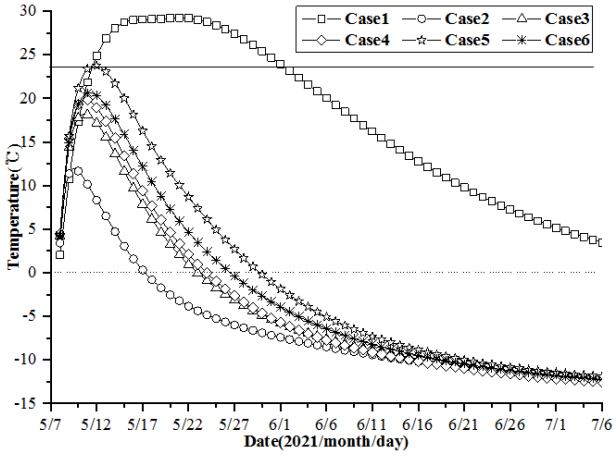

(b) Temperature difference between center and surface

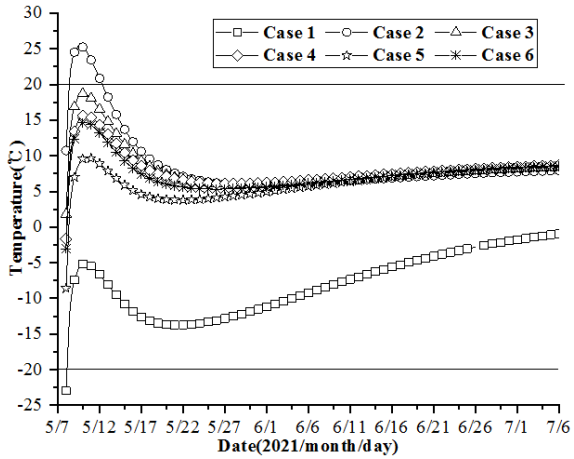

(c) Temperature difference between neighboring layers

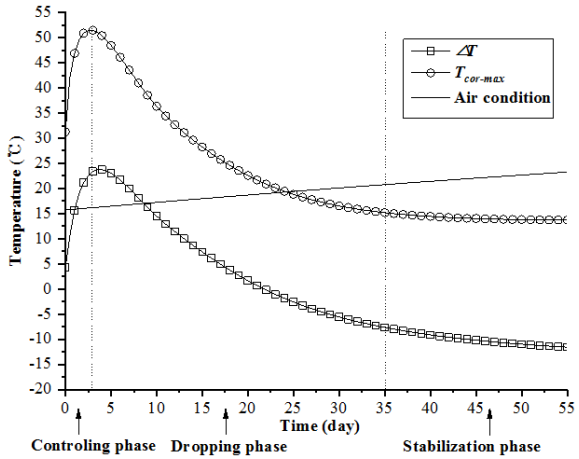

(d) Target temperature control curves

Fig. 10 Target temperature control curves

neighbouring layers are 18.57°C and 14.65°C, respectively. Both cases can meet the temperature control requirements. The cooling duration is 30 days and 40 days for Cases 3 and 6, respectively. Case 3 is selected as the implementation design for the target temperature control curve.

Two target temperature control curves show the maximum temperature at the center of the concrete block and the temperature difference between the center and surface change with time. As aforementioned, the cooling process is divided into three phases of temperature controlling, dropping and stabilization. The pouring temperature is set as 28°C, which reduces the pre-cooling cost compared to 7°C to 10°C in typical engineering practices. The peak temperature is 65°C, which has a safety margin of 10°C compared to the design requirement of 75°C and the temperature difference between the center and surface is 23.5°C. The duration of the dropping phase is extended to 30 days, so as to achieve a continuous and smooth cooling process.

4.4 Performance of ICCS

The performance of ICCS was evaluated from three aspects: the effectiveness, safety reliability, and technical feasibility.

In terms of the effectiveness, there are no structural cracks in the construction site, and the critical monitoring indicators and the field monitoring data are evaluated. A partial period monitoring data of concrete #8 exported by the system are shown in Fig. 11. The maximum central temperature reached 57.7°C, occurring at a curing age of 5 days post-pouring. The maximum temperature difference between the center and surface was essentially synchronous with the peak center temperature, with the temperature difference being less than 25°C after 9 days. During the stable phase, the temperature difference was already below 10°C. Overall, the maximum center temperature controlled was below the regulatory standard of 75°C, the center-surface temperature difference was lower than the regulatory requirement of 20°C, the temperature difference between neighbouring layers was approximately 3.2°C from the completion of pouring to the end of monitoring. Overall, the fluctuation range of the temperature and flow curves under the LSTM control algorithm is significantly smaller than that of the manual adjustment. The curves are smoother, which is helpful for the control of a smaller temperature gradient and can meet the requirements of the concrete temperature control for bridges.

The index of the control deviation is relatively high, reaching 96.4%. The maximum temperature curve is continuous and smooth, slightly below the target temperature control curve. The mean temperature is 62.3°C, occurring at 2.17 days (or 52 hrs) after the concrete placement. With the influence of solar radiation, the temperature difference between the centre and the surface fluctuates slightly. The temperature difference is less than 15°C and meets the requirements. The temperature drop rate varies from 1.5°C/d to 1.8°C/d. The pouring temperature of the three loops ranges from 14°C to 16°C. The water flow rate ranges from 20 L/min to 70 L/min. The trained LSTM model is used to forecast the recommended flow rates at 23 days (142 time-steps). The average error between the recommended and actual flow is only 3.5 L/min, showing that the data training is successful (Fig. 12).

The direct economic benefit is to reduce the concrete curing cost by approximately 90% in terms of the safety reliability. The indirect economic benefits also contribute significantly, including shortening the construction progress about 2 months and reducing the safety risks in complex construction sites.

In terms of the technical feasibility, the system is modularized, standardized and integrated. It is featured by

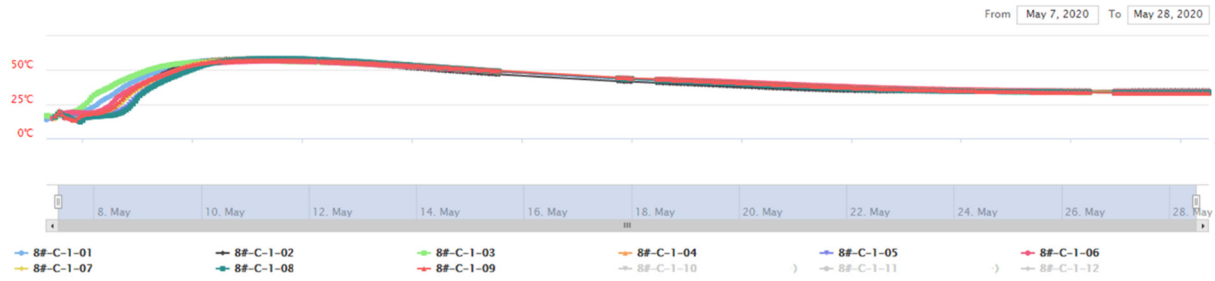

(a) Temperature change of central concrete

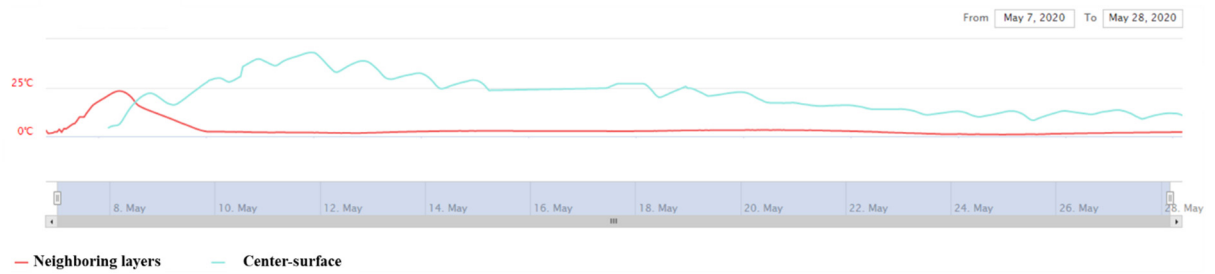

(b) Temperature difference

Fig. 11 Temperature curves of ICCS monitoring

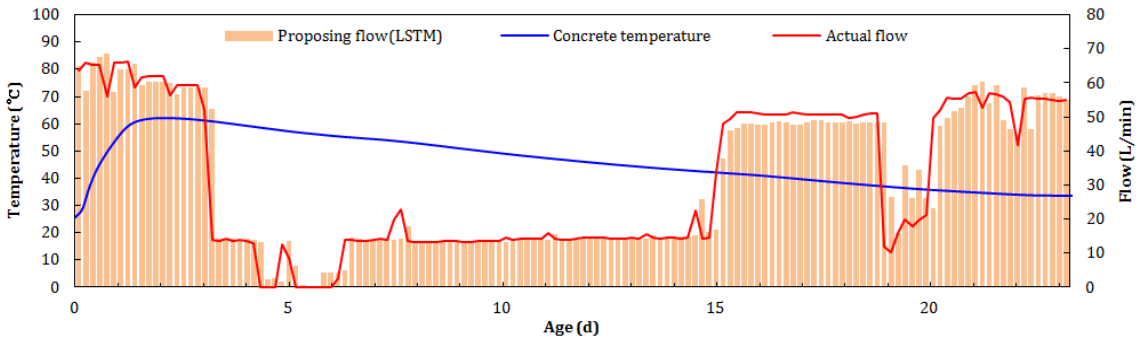

Fig. 12 Comparison of flow recommended and actual flow controlled by ICCS

the configuration regulation, complex environmental adaptability, and remote control, which is suitable for the construction of complex infrastructure projects in harsh environments. The system has been applied to other bridges and dams.

5. Conclusions

Mass concretes have nowadays been widely used to construct bridges, dams and buildings at an unprecedented level. However, it has been a great challenge to control the cracking of the mass concretes. In this study, an ICCS was developed to control the cracking of the mass concrete during the construction of a bridge. The ICCS consists of a hardware system, a control algorithm based on the neural networks of long short-term memory (LSTM) and a proportional-integral-derivative (PID) controller, and an information management system. The ICCS collects data from multiple sources and adjusts the water temperature and flow in the cooling system according to the hydration heat of concrete so as to prevent concrete cracking. Moreover, the monitoring data in the ICCS can be accessed by users to facilitate the project management.

A continuous cooling control strategy was proposed using the LSTM and PID algorithms for on-site intelligent cooling control during the concrete placing and curing. The innovative control algorithm enables the dynamic coupling of the flow and cooling temperature and ensures that the ICCS runs with high accuracies and stabilities under unsupervised learning conditions. The LSTM maps the comprehensive temperatures and flows in the monitoring system to the flow indicators in the regulating system. With online learning and adjustment, the PID controller ensures the high precision and stable operation of the ICCS. The initial value of the neural network weight is determined based on a large amount of data.

The ICCS with the control strategy is applied to mitigate the cracking of mass concretes during the construction of the Sylla Mu Lun Grand Bridge. The results showed that, with the implementation of the ICCS, both the real-time concrete temperature curves and the key indexes met the design requirements. Therefore, the reliability, cost efficiency, and technical feasibility of the ICCS together with the control strategy have been verified, which can provide references for the design and construction of similar projects involving in the mass concretes.

Acknowledgments

The research described in this paper was financially supported by Road & Bridge International Huabei Co., Ltd (Grant No. ZJLJ-JWGSXM-JSFW-2019-003), the China Three Gorges Corporation (No: WDD/0578) Snohydro Bureau 11 Co LTD's Management Department of the Julius Nyerere Hydropower Station Project in the United Republic of Tanzania (Grant No. SHC-JNHPP-JSFW-01-18012022) and Management Department of the Kafue Gorge Lower Hydropower Station Project in Zambia (Grant No. SH-KGL-SUB-2021003). The authors would like to express their gratitude for the financial support that made this study possible.

References

American Road & Transportation Builders Association (2021), "2021 Bridge Conditions Report", American Road & Transportation Builders Association, Washington D.C., USA.

An, G., Yang, N., Li, Q., Hu, Y. and Yang, H. (2020), "A simplified method for real-time prediction of temperature in mass concrete at early age", *Appl. Sci.*, **13**(10), 4451. https://doi.org/10.3390/app10134451

An, R.N., Lin, P., Li, Z.C., Zhang, L.B., Cheng, F., Xia, Y., Liu, Y. and Liu, H.Y. (2024), "Intelligent ventilation-on-demand control system for the construction of underground tunnel complex", *J. Intell. Constr.*, **2**, 9180032. https://doi.org/10.26599/JIC.2024.9180032

Azenha, M., Lameiras, R., de Sousa, C. and Barros, J. (2014), "Application of air cooled pipes for reduction of early age cracking risk in a massive RC wall", *Eng. Struct.*, **62-63**, 148-163. https://doi.org/10.1016/j.engstruct.2014.01.018

Bentz, D.P., Waller, V. and de Larrard, F. (1998), "Prediction of adiabatic temperature rise in conventional and high-performance concretes using a 3-D microstructural model", *Cemram. Concrete Res.*, **28**(2), 285-297. https://doi.org/10.1016/S0008-8846(97)00264-0

Chorzepa, M.G., Hamid, H., Durham, S.A. and Goode, L. (2018), "Analysis of cracking caused by hydration heat in bridge seals utilizing innovative massive concrete mixtures", In: *Structures Congress 2018*, April.

Chuc, N.T., Don, L.Q., Thoan, P.V. and Kiet, B.A. (2018), "The effects of insulation thickness on temperature field and evaluating cracking in the mass concrete", *Electr. J. Struct. Eng.*, **18**(2), 128-132. https://doi.org/10.56748/ejse.182722

Conceicao, J., Faria, R., Azenha, M. and Miranda, M. (2020), "A new method based on equivalent surfaces for simulation of the post-cooling in concrete arch dams during construction", *Eng.*

Struct., **209**, 109976. https://doi.org/10.1016/j.engstruct.2019.109976

Crowley, A.M. (2015), "The Development of a Lower Heat Concrete Mixture for Mass Concrete Placement Conditions", Ph.D. Dissertation; Tennessee Technological University, TN, USA.

Dias, I.F., Oliver, J., Lemos, J.V. and Lloberas-Valls, O. (2016), "Modeling tensile crack propagation in concrete gravity dams via crack-path-field and strain injection techniques", *Eng*. *Fract*. *Mech*., **154**, 288-310. https://doi.org/10.1016/j.engfracmech.2015.12.028

Djamila, B., Othmane, B., Said, K. and El-Hadj, K. (2018), "Combined effect of mineral admixture and curing temperature on mechanical behavior and porosity of SCC", *Adv*. *Concrete Constr*., *Int*. *J*., **6**(1), 69-85. https://doi.org/10.12989/acc.2018.6.1.069

Do, T.A. (2015), "Influence of footing dimensions on early-age temperature development and cracking in concrete footings", *J*. *Bridge Eng*., **20**(3), 6014007. https://doi.org/10.1061/(ASCE)BE.1943-5592.0000690

Do, T.A., Lawrence, A.M., Tia, M. and Bergin, M.J. (2014), "Determination of required insulation for preventing early-age cracking in mass concrete footings", *Transport Res*. *Rec*., **2441**(1), 91-97. https://doi.org/10.3141/2441-12

Feng, C., Chang, L., Li, C., Ding, T. and Mai, Z. (2019), "Controller optimization approach using LSTM-based identification model for pumped-storage units", *IEEE Access*, **7**, 32714-32727. https://doi.org/10.1109/ACCESS.2019.2903124

García, A., Lura, P., Partl, M.N. and Jerjen, I. (2013), "Influence of cement content and environmental humidity on asphalt emulsion and cement composites performance", *Mater*. *Struct*., **46**(8), 1275-1289. https://doi.org/10.1617/s11527-012-9971-6

Gilliland, J.A. and Dilger, W.H. (1997), "Monitoring concrete temperature during construction of the Confederation Bridge: The Confederation Bridge", *Can*. *J*. *Civil Eng*., **24**(6), 941-950. https://doi.org/1.1139/CJCE-24-6-941

Huang, Y.H., Liu, G.X., Huang, S.P., Rao, R. and Hu, C.F. (2018), "Experimental and finite element investigations on the temperature field of a massive bridge pier caused by the hydration heat of concrete", *Constr*. *Build*. *Mater*., **192**, 240-252. https://doi.org/10.1016/j.conbuildmat.2018.10.128

Kang, F., Li, J. and Dai, J. (2019), "Prediction of long-term temperature effect in structural health monitoring of concrete dams using support vector machines with Jaya optimizer and salp swarm algorithms", *Adv*. *Eng*. *Softw*., **131**, 60-76. https://doi.org/10.1016/j.advengsoft.2019.03.003

Khan, M. and Ali, M. (2016), "Use of glass and nylon fibers in concrete for controlling early age micro cracking in bridge decks", *Constr*. *Build*. *Mater*., **125**, 800-808. https://doi.org/10.1016/j.conbuildmat.2016.08.111

Khandel, O., Soliman, M., Floyd, R.W. and Murray, C.D. (2021), "Performance assessment of prestressed concrete bridge girders using fiber optic sensors and artificial neural networks", *Struct*. *Infrastr*. *Eng*., **17**(5), 605-619. https://doi.org/10.1080/15732479.2020.1759658

Kim, J.K. and Kim, K.H. (1992), "Thermal stress analysis for the heat of hydration considering creep and shrinkage effects in mass concrete", *J*. *Korea Concr*. *Inst*., **4**(3), 101-111.

Kim, K,-H., Jeon, S.-E., Kim, J.K. and Yang, S. (2003), "An experimental study on thermal conductivity of concrete", *Cement Concrete Res*., **33**(3), 363-371. https://doi.org/10.1016/S0008-8846(02)00965-1

Krauss, P.D. and Rogalla, E.A. (1996), "Transverse Cracking in Newly Constructed Bridge Decks (NCHRP Report 380)", Transportation Research Board & National Research Council, Washington, D.C., USA.

Lawson, L., Ryan, K.L. and Buckle, I.G. (2020), "Bridge temperature profiles revisited: thermal analyses based on recent meteorological data from Nevada", *J*. *Bridge Eng*., **25**(1), 4019124. https://doi.org/10.1061/(ASCE)BE.1943-5592.0001498

Li, Y., Nie, L. and Wang, B. (2014), "A numerical simulation of the temperature cracking propagation process when pouring mass concrete", *Autom*. *Constr*., **37**, 203-210 https://doi.org/10.1016/J.AUTCON.2013.08.005

Li, M., Lin, P., Chen, D.X., Li, Z.,C., Liu, K. and Tan, Y.S. (2023), "An ANN based short-term temperature forecast model for mass concrete cooling control", *J*. *Tsinghua Univ*. (*Sci*. *& Technol*.), **28**(3), 511-524. https://doi.org/10.26599/TST.2022.9010015

Li, P.F., Wang, H.Y., Nie, D., Wang, D.Y. and Wang, C.Z. (2023), "A method to analyze the long-term durability performance of underground reinforced concrete culvert structures under coupled mechanical and environmental loads", *J*. *Intell*. *Constr*., **1**, 9180011. https://doi.org/10.26599/1c.2023.9180011

Lin, P., Li, Q.B., Zhou, S.W. and Hu, Y. (2013), "Intelligent cooling control method and system for mass concrete", *J*. *Hydr*. *Eng*., **44**(8), 950-957. [in Chinese]

Lin, P., Peng, H.Y., Fan, Q.X., Xiang, Y.F., Yang, Z. and Yang, N. (2021), "A 3D thermal field restructuring method for concrete dams based on real-time temperature monitoring", *KSCE J*. *Civil Eng*., **25**(4), 1326-1340. https://doi.org/10.1007/s12205-021-1084-8

Miao, P.Y., Yokota, H. and Zhang, Y.F. (2023), "Deterioration prediction of existing concrete bridges using a LSTM recurrent neural network", *Struct*. *Infrastr*. *Eng*., **19**(4), 475-489. https://doi.org/10.1080/15732479.2021.1951778

Mohammadikia, R. and Aliasghary, M. (2019), "A fractional order fuzzy PID for load frequency control of four-area interconnected power system using biogeography-based optimization", *Int*. *T*. *Electr*. *Energy*, **29**(2), e2735. https://doi.org/10.1002/etep.2735

Ng, P.L., Chen, J.J. and Kwan, A.K.H. (2017), "Adiabatic temperature rise of concrete with limestone fines added as a filler", *Procedia Eng*., **172**, 768-775. https://doi.org/10.1016/j.proeng.2017.02.121

Nguyen, T., Huynh, T. and Tang, V. (2019), "Prevention of crack formation in massive concrete at an early age by cooling pipe system", *Asian J*. *Civil Eng*., **20**(8), 1101-1107. https://doi.org/10.1007/s42107-019-00175-5

Ning, Z.Y., Lin, P., Ouyang J.S., Yang, Z.L., He, M.W. and Ma, F.P. (2022), "Intelligent cooling control for mass concrete relating to spiral case structure", *Adv*. *Concrete Constr*., *Int*. *J*., **14**(1), 57-70. https://doi.org/10.12989/acc.2022.14.1.057

Pearson, C. and Delatte, N. (2006), "Collapse of the Quebec Bridge, 1907", *J*. *Perform*. *Constr*. *Facil*., **20**(1), 84-91. https://doi.org/10.1061/(ASCE)0887-3828(2006)20:1(84)

Peng, H., Lin, P., Xiang, Y., Chen, W., Zhou, S., Yang, N. and Qiao, Y. (2020), "A positioning method of temperature sensors for monitoring dam global thermal field", *Front*. *Mater*., **7**, 587738. https://doi.org/10.3389/fmats.2020.587738

Remond, S. and Pizette, P. (2014), "A DEM hard-core soft-shell model for the simulation of concrete flow", *Cem*. *Concrete Res*., **58**, 169-178. https://doi.org/10.1016/j.cemconres.2014.01.022

Sahani, A.K., Samanta, A.K. and Roy, D.K. (2019), "SInfluence of mineral by-products on compressive strength and microstructure of concrete at high temperature", *Adv*. *Concrete Constr*., *Int*. *J*., **7**(4), 263-275. https://doi.org/10.12989/acc.2019.7.4.263

Sargam, Y., Faytarouni, M., Riding, K., Wang, K., Jahren, C. and Shen, J. (2019), "Predicting thermal performance of a mass concrete foundation -A field monitoring case study", *Case Stud*. *Constr*. *Mater*., **11**, e289. https://doi.org/10.1016/j.cscm.2019.e00289

Semendary, A.A., Steinberg, E.P., Walsh, K.K. and Barnard, E. (2019), "Effects of temperature distributions on thermally induced behavior of UHPC shear key connections of an

adjacent precast prestressed concrete box beam bridge", *J. Bridge Eng*., **24**(2), 4018115. https://doi.org/10.1061/(ASCE)BE.1943-5592.0001346

Seo, T., Kim, S. and Lim, C. (2015), "Experimental study on hydration heat control of mass concrete by vertical pipe cooling method", *J. Asian Architect. Build*., **14**(3), 657-662. https://doi.org/10.3130/jaabe.14.657

Song, X., Melhem, H., Li, J., Xu, Q. and Cheng, L. (2016), "Effects of solar temperature gradient on long-span concrete box girder during cantilever construction", *J. Bridge Eng*., **21**(3), 4015061. https://doi.org/10.1061/(ASCE)BE.1943-5592.0000844

Song, C.J., Zhang, G., Wen, H. and Zhang, Y.F. (2020), "Effect of pipe-cooling system on thermal-mechanical behaviour of PC box bridge girders at hydration age", *ABEN*, **1**, 9. https://doi.org/10.1186/s43251-020-00009-4

Subramaniam, K.V., Kunin, J., Curtis, R. and Streeter, D. (2010), "Influence of early temperature rise on movements and stress development in concrete decks", *J. Bridge Eng*., **15**(1), 108-116. https://doi.org/10.1061/(ASCE)1084-0702(2010)15:1(108)

Sun, X.J., Wang, S.Q., Jin, J.P., Wang, Z. and Gong, F.Y. (2023), "Computational methods of mass transport in concrete under stress and crack conditions: A review", *J. Intell. Constr*., **1**, 9180015. https://doi.org/10.26599/JIC.2023.9180015

Tatro, S.B. and Schrader, E.K. (1985), "Thermal considerations for roller-compacted concrete", *J. Proceedings*, **82**(2), 119-128. https://doi.org/10.14359/10319

Vytenis, B. (1994), "Fire Safety Design and Concrete", *Fire Safety J*., **23**(4), 439-442. https://doi.org/10.1016/0379-7112(94)90007-8

Wu, X.G., Yu, S.Y., Tao, X.K., Chen, B.C., Liu, H., Yang, M. and Thomas, H.K. (2020), "Behavior of UHPC-RW-RC wall panel under various temperature and humidity conditions", *Adv. Concrete Constr*., *Int. J*., **9**(5), 459-467. https://doi.org/10.12989/acc.2020.9.5.459

Yu, X.Z., Chen, J.Y., Xu, Q. and Zhi, Z. (2018), "Research on the influence factors of thermal cracking in mass concrete by model experiments", *KSCE J. Civ. Eng*., **22**(8), 2906-2915. https://doi.org/10.1007/s12205-017-2711-2

Zhang, Y., Zhu, Y.P., Ma, P.F., He, S.L. and Shao, X.D. (2023), "Effect of ages and season temperatures on bi-surface shear behavior of HESUHPC-NSC composite", *Adv. Concrete Const*., *Int. J*., **15**(6), 359-376. https://doi.org/10.12989/acc.2023.15.6.359

Zhu, Y.P., Zhang, Y., Hussein, H.H., Qiu, M.H., Meng, D.L. and Chen, G. (2022), "Flexural strengthening of large-scale damaged reinforced concrete bridge slab using UHPC layer with different interface techniques", *Struct. Infrastr. E*., **18**(6), 879-892. https://doi.org/10.1080/15732479.2021.1876104